The Astrophysical Journal, 744:16 (8pp), 2012 January 1 doi:10.1088/0004-637X/744/1/16

THE RICH CIRCUMSTELLAR CHEMISTRY OF SMP LMC 11

S. E. Malek[1], J. Cami[1,2], and J. Bernard-Salas[3]
[1] Department of Physics and Astronomy, University of Western Ontario, London, ON N6A 3K7, Canada; smalek2@uwo.ca
[2] SETI Institute, 189 Bernardo Avenue, Suite 100, Mountain View, CA 94043, USA; jcami@uwo.ca
[3] Institut d'Astrophysique Spatiale, CNRS/Universite Paris-Sud 11, 91405 Orsay, France
Received 2011 July 11; accepted 2011 November 2; published 2011 December 7

ABSTRACT

Carbon-rich evolved stars from the asymptotic giant branch to the planetary nebula phase are characterized by a rich and complex carbon chemistry in their circumstellar envelopes. A peculiar object is the preplanetary nebula SMP LMC 11, whose *Spitzer* Infrared Spectrograph spectrum shows remarkable and diverse molecular absorption bands. To study how the molecular composition in this object compares to our current understanding of circumstellar carbon chemistry, we modeled this molecular absorption. We find high abundances for a number of molecules, perhaps most notably benzene. We also confirm the presence of propyne (CH_3C_2H) in this spectrum. Of all the cyanopolyynes, only HC_3N is evident; we can detect at best a marginal presence of HCN. From comparisons to various chemical models, we can conclude that SMP LMC 11 must have an unusual circumstellar environment (a torus rather than an outflow).

Key words: astrochemistry – circumstellar matter – stars: AGB and post-AGB – stars: carbon – stars: individual (SMP LMC 11)

Online-only material: color figures

1. INTRODUCTION

As stars with initial masses between 0.8 and 8–9 $M_\odot$ approach the end of their lives, they reach the asymptotic giant branch (AGB) stage. The AGB is characterized by alternate hydrogen and helium shell burning, dredge-up events, and extreme mass-loss rates (up to $10^{-4}\,M_\odot$ yr^{-1}; Iben & Renzini 1983). This high mass loss causes the star to evolve further, leaving the AGB. When a star leaves the AGB it may become what is known as a preplanetary nebula (pPN) during a relatively short-lived (lasting $\sim 10^3$–10^4 yr; Vassiliadis & Wood 1994) transitionary period before becoming a planetary nebula (PN).

The material lost by a star during its time on the AGB goes into the circumstellar environment (CSE) before it is dispersed into the interstellar medium (ISM). The CSE is a relatively cool region (with temperatures lower than the effective temperatures of AGB stars, where $T_{\rm eff} \approx 3000$ K), which allows the formation of molecules and dust beginning on the AGB and continuing into the (p)PN stages.

One of the first and most stable molecules to form in the CSE is CO. As a result, the relative amounts of carbon and oxygen in the CSE largely determine future chemistry. Stars begin their lives with more oxygen than carbon (C/O < 1), but depending on the initial stellar mass and metallicity, an AGB star may undergo sufficient dredge-up events and become carbon-rich (C/O > 1), resulting in what is known as a carbon star (or a carbon-rich star).

The chemistry of carbon stars can result in an assortment of molecules due to the ability of carbon to form a variety of chemical bonds. For example, more than 60 molecules have been detected in the CSE of the prototypical carbon-rich AGB star IRC+10216 (e.g., Cernicharo et al. 1996).

The carbon chemistry in the CSE of AGB stars and (p)PNe is also of particular interest because a group of molecules known as polycyclic aromatic hydrocarbons (PAHs) are thought to form here (Latter 1991). These molecules are ubiquitous in the universe with up to 10%–15% of cosmic carbon contained in PAHs (Snow & Witt 1995).

In the current models of PAH formation, benzene (C_6H_6) formation is considered a bottleneck step (Frenklach & Feigelson 1989; Cherchneff et al. 1992).

Not much is known about the formation of benzene in the CSEs of evolved stars, although there are chemical models describing its formation in the inner shocked regions of the CSE surrounding AGB stars (Cherchneff et al. 1992) as well as through photochemical reactions in the CSE of pPNe (Woods et al. 2002, 2003).

While PAHs are ubiquitous in the universe (including carbon-rich PNe), benzene is not often found in evolved stars; it has been found in just two objects thus far: CRL 618 (Cernicharo et al. 2001b) and SMP LMC 11 (Bernard-Salas et al. 2006, hereafter Paper I). This suggests that it is either difficult to form or that it reacts quickly once formed.

In this paper, we will discuss the latter object, SMP LMC 11, which is a carbon-rich pPN in the Large Magellanic Cloud. It is described as a low-excitation pPN (Sanduleak et al. 1978; Morgan 1984) and has a bipolar outflow (Shaw et al. 2006). It also shows a rather high expansion velocity (122 km s^{-1}; Dopita et al. 1988) with multiple velocity components.

Here we present a detailed analysis of the molecular absorption bands in the mid-infrared spectrum of SMP LMC 11 (first presented in Paper I) and show that our results are inconsistent with current models for the chemistry in evolved carbon-rich CSEs.

We begin this paper with a description of the observations and data reduction in Section 2, then we describe the dust continuum in Section 3. We follow this with an inventory of the molecular bands in the spectrum and the method we use to model these bands in Section 4. We then present our results from our model fits in Section 5. Next, we discuss the implications of our results for the evolutionary status, chemical evolution, and geometry of

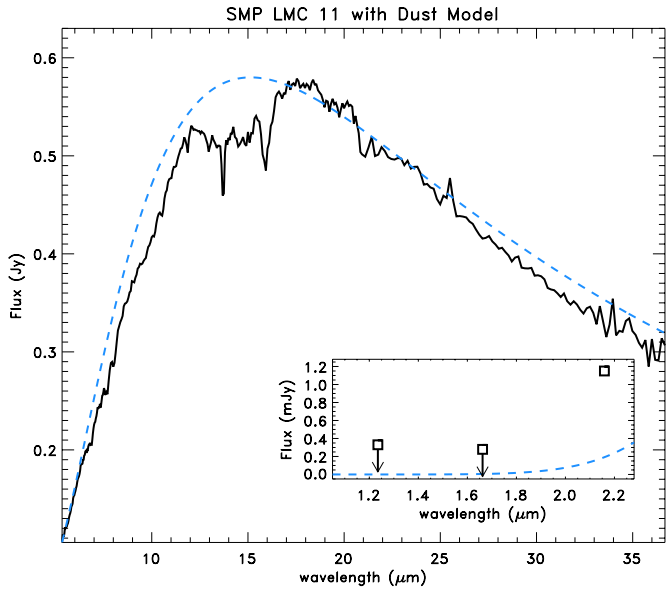

Figure 1. *Spitzer*–IRS low-resolution spectrum (SL and LL combined) of SMP LMC 11 (black) and a dust model (dashed gray or dashed blue line in the online version). The inset shows the 2MASS fluxes with the dust model.

(A color version of this figure is available in the online journal.)

SMP LMC 11 in Section 6. Finally, we present our conclusions in Section 7.

2. OBSERVATIONS AND DATA REDUCTION

SMP LMC 11 was observed with the *Spitzer Space Telescope* (Werner et al. 2004) Infrared Spectrograph (IRS; Houck et al. 2004) as part of the Guaranteed Time Observer (GTO) program on 2005 June 6 (program ID 103, AOR key 4947712). Here we present a new reduction of the spectrum with the latest calibration files (pipeline version S18.18). We obtained the basic calibrated data (BCD) files for SMP LMC 11 and processed the data for the short high (SH, $R = 600$, $\lambda = 9.9$–$19.6\,\mu$m), short low (SL, $R = 60$–127, $\lambda = 5.2$–$14.5\,\mu$m), and long low (LL, $R = 57$–126, $\lambda = 14.0$–$38.0\,\mu$m) modes.

We cleaned the data using IRSCLEAN with the campaign rogue pixel mask and extracted it in SMART v8.2.1 (Higdon et al. 2004); we extracted the SH data using full aperture extraction, and the SL and LL data with the manual optimal extraction mode (Lebouteiller et al. 2010). Next we defringed the LL mode and trimmed the edges of the orders for all modules to remove edge effects. We eliminated flux jumps between the orders by comparing the overlap regions and scaling the orders (for the SH, orders were scaled to match order 20, for the low-resolution data SL2 was scaled to SL1 and both were scaled to the LL data), then we averaged the flux from the two nod positions. Since we were unsure of the reliability of the initial uncertainty estimates, we instead estimated the uncertainties on the flux values by measuring the standard deviation in a featureless region of the SH spectrum between 16.53 and 17.44 μm; we found a standard deviation of 0.0122 Jy, corresponding to a signal-to-noise ratio (S/N) of 47 in this range.

Finally, to facilitate comparison to molecular models, we shifted the spectrum to the rest frame using a radial velocity of 263.5 km s^{-1} (Morgan & Parker 1998) and the relative motion of *Spitzer* at the time of the observations ($V_{\rm LSR} = 12.5$ km s^{-1}). The full low-resolution spectrum is shown in Figure 1.

3. THE DUST CONTINUUM

Figure 1 shows the *Spitzer*–IRS continuum as well as the Two Micron All Sky Survey (2MASS; Skrutskie et al. 2006) *H*-, *J*-, and *K*-band fluxes (Cutri et al. 2003). From those data, it seems clear that there is no appreciable stellar continuum that could contribute to the mid-IR emission. We thus conclude that the flux in the entire IRS spectrum is dominated by dust emission.

The region beyond 17 μm has a few apparent features near 19 and 21 μm in the LL data. However, as these features are absent from a quick reduction of the long high (LH, $R = 600$, $\lambda = 18.7$–$37.2\,\mu$m) data, we consider these to be artifacts. Thus, the dust emission does not show clear spectral features, and thus is presumably caused by amorphous carbon dust.

Since it is precisely this dust emission that is then absorbed by molecular bands (especially in the 10–17 μm region, see Figure 1), we require some idea about the properties of this dust continuum before we can model the molecular bands. A single blackbody curve cannot properly reproduce the overall shape of the dust continuum, suggesting that there is some stratification in the dust layers. From our point of view, we can see through the outer (and colder) dust layers up the point where the dust becomes optically thick; at that point, the dust temperature is $T_{\rm d}^{\rm max}$. We thus approximated the dust emission by a weighted sum of blackbody spectra at temperatures between $T_{\rm d}^{\rm max}$ and an arbitrarily chosen minimum temperature $T_{\rm d}^{\rm min}$ of 25 K in steps of 25 K. Assuming optically thin dust in radiative equilibrium with the hottest (optically thick) dust, we then determined the appropriate weights for each temperature bin consistent with a constant-velocity outflow at a constant mass-loss rate (i.e., we determined the mass in each layer). We find that the best model is one with a maximum dust temperature of about 425 K (see Figure 1). However, even in such a case, we overestimate the dust emission at the longer wavelengths; this suggests that there is less cold dust than expected for a constant-velocity outflow at a constant mass-loss rate. Nonetheless, the cold dust does not matter much for the analysis of the molecular bands; for the modeling presented in this paper, we assume that the molecules are absorbing 425 K blackbody radiation.

We also note that our dust temperature estimate is higher than that in Paper I, but our estimate should be more reliable than their graybody fit.

4. MOLECULAR BANDS

4.1. Molecular Inventory

Superposed on the dust emission are many absorption features due to various molecular species (see Figure 2). We will restrict our discussion to wavelengths shorter than 17 μm, where most of the absorption occurs.

Here, we describe the molecular bands in great detail and determine the physical conditions by modeling these bands.

Acetylene (C_2H_2) is often the dominant molecular absorber in the infrared spectra of carbon-rich pPNe. In the spectrum of SMP LMC 11, C_2H_2 provides by far the strongest absorption. The *Q*-branch for the ν_5 bending mode is obvious as a very deep absorption feature at 13.7 μm; additionally, the *P*- and *R*-branches of C_2H_2 cause much of the broad and deep absorption that is obvious between 12 and 16 μm (see Figure 1). Such broad and deep C_2H_2 absorption is also seen in some other carbon-rich objects, such as the carbon star IRAS 04496−6958 (Speck et al. 2006), for example. In addition, acetylene exhibits a much weaker combination band (ν_4+ν_5) at 7.5 μm which is blended with other features in the spectrum of SMP LMC 11.

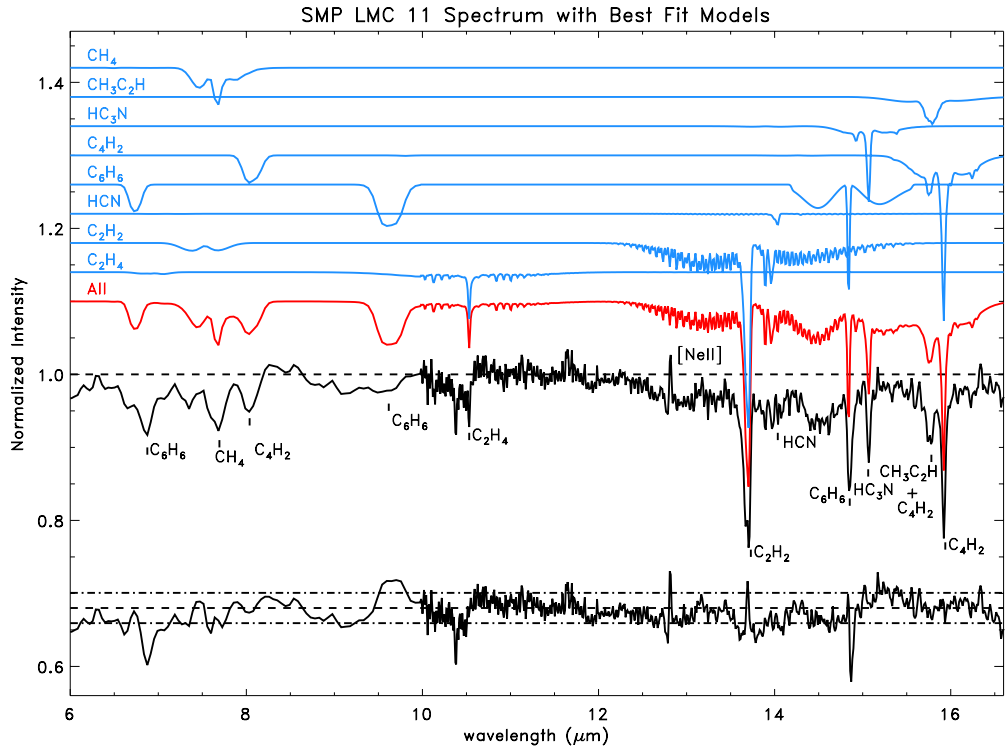

Figure 2. Normalized SL and SH spectra for SMP LMC 11 from 6 to 16.6 μm with our best-fit models and residuals. The combined best fit is shown offset above the spectrum in dark gray (red in the online version). The individual best fits for each molecule are offset above this in light gray (blue). The residuals are shown offset below the spectrum and the dot-dashed lines indicate the error ranges.

(A color version of this figure is available in the online journal.)

Larger acetylene chains are less commonly observed in the CSE of pPNe (Fonfría et al. 2011). In the spectrum of SMP LMC 11 though diacetylene (C_4H_2) is another major contributor to the molecular absorption in the spectrum. The ν_8 bending mode of this species appears at 15.9 μm and the $\nu_6 + \nu_8$ combination band is clearly visible at ~8 μm. Small amounts of the corresponding ν_{11} bending mode of triacetylene (C_6H_2) might be present in the red wing of the 15.9 μm feature.

In contrast, HCN—which often shows up in carbon star spectra alongside the C_2H_2 band at 14 μm—at best barely contributes to the absorption in this spectrum. It is thus surprising that HC_3N is present and shows a clear and deep absorption at 15.03 μm from its bending mode. There is no evidence for any longer cyanopolyynes; for instance, there is no absorption at 15.57 μm from the ν_7 band of HC_5N.

Nearly unique for pPNe (with one other detection thus far in CRL 618; see Cernicharo et al. 2001b), the spectrum also shows significant benzene absorption (as noted in Paper I). It has its deepest absorption at 14.85 μm, where the ν_4 bending mode absorbs more than 15% of the total continuum flux. Additionally, strong absorption is clearly present at the wavelengths where other strong benzene bands are expected: another bending mode (ν_{14}) at 9.6 μm and a ring stretching and deforming mode (ν_{13}) at 6.72 μm.

In the blue wing of the C_4H_2 band, near 15.78 μm, some additional absorption could be due to the ν_8 bending mode of propyne (CH_3C_2H, also sometimes called methylacetylene) at 15.78 μm, as suggested in Paper I. Furthermore, there is also some absorption visible in the spectrum from the ν_4 band of CH_4 at 7.7 μm as well as the ν_7 band of C_2H_4 at 10.53 μm. Finally, we could not determine the origin of the absorption feature near 10.38 μm, although we suspect a molecular origin for this feature.

4.2. Modeling the Molecular Absorption

We modeled the molecular absorption using the same methods that are used to build the SpectraFactory database (Cami et al. 2010). These model calculations start from line lists detailing the frequencies and intensities of the individual molecular transitions.

Line lists for C_2H_2 (including the $H^{13}CCH$ isotopologue), HCN, CH_4, and C_2H_4 are taken from the HITRAN 2008 database (Rothman et al. 2009); the line lists for C_4H_2, C_6H_6, HC_3N, and CH_3C_2H are from the GEISA database (Jacquinet-Husson et al. 2008).

As we could not find reliable line lists for all species or bands, we calculated some line lists from molecular constants and PGOPHER v 7.1.108 (Western 2010). The GEISA line list for benzene contains only data for the fundamental ν_4 band. Thus, in order to model benzene absorption at the shorter wavelengths in the SL data, we calculated line lists for the ν_{13} and ν_{14} bands using molecular constants from Dang-Nhu & Plíva (1989). Similarly, the GEISA line list for C_4H_2 does not contain data for the transitions of the $\nu_6 + \nu_8$ combination band at ~8 μm; we thus calculated a line list using molecular constants found in Arié & Johns (1992), Guelachvili et al. (1984), and Khlifi et al. (1995). Finally, we calculated a C_6H_2 list using data from McNaughton & Bruget (1991).

From these line lists, we calculated optical depths assuming a population in local thermodynamic equilibrium and a Gaussian intrinsic line profile with a width of 10 km s^{-1}, which is typical of outflows of evolved stars. We carried out radiative transfer through isothermal, plane-parallel molecular slabs in front of a 425 K blackbody background (see Section 3) and smoothed and rebinned the resulting models to match the resolving power of the observations—600 for the SH module and 90 for the SL data.

Table 1
Temperatures and Column Densities for the Best Model Fits to our Data as well as Nominal 1σ Uncertainties

Molecule	log N	T (K)
C_2H_4	$17.30^{+0.05}_{-0.50}$	350^{+50}_{-50}
C_2H_2	$18.10^{+0.05}_{-0.05}$	
$H^{13}CCH$	$16.90^{+0.10}_{-0.10}$	375^{+25}_{-50}
HCN	$16.50_{-1.50}$	
C_6H_6	$17.80^{+0.40}_{-1.00}$	350^{+50}_{-50}
C_4H_2	$17.10^{+0.05}_{-0.05}$	
CH_3C_2H	$17.00^{+0.10}_{-0.05}$	$325^{+12.5}_{-25}$
HC_3N	$16.40^{+0.10}_{-0.05}$	
CH_4	$17.80^{+0.70}_{-0.20}$	$250^{+150}_{-12.5}$

We compared the resulting models to the observations (normalized by a cubic spline continuum) and calculated χ^2_ν, the reduced χ^2 statistic. However, we note that there may be some systematic errors as well. For instance, it is important to realize that the current line lists for C_2H_2 do not allow us to reproduce the broad and deep absorption in the 12–16 μm range (see Speck et al. 2006, for a discussion).

To find the best model, we calculated models at different temperatures ranging from 200 to 400 K with a step size of 25 K, and similarly at column densities between $N = 10^{15}$ and $N = 10^{19}$ cm^{-2} in steps of log $N = 0.1$ and then calculated the χ^2_ν value for each model. For wavelength ranges containing absorption due to several species, we properly treated line overlap by summing the optical depth profiles for each contributing molecule prior to performing the radiative transfer calculations when we fit several species simultaneously. We thus simultaneously modeled the absorption of the C_2H_2 isotopologues and HCN between 12 and 14 μm and similarly also combined C_4H_2, C_6H_2, CH_3C_2H, and HC_3N in the 15–16.5 μm range. We fit benzene to the spectrum between 14.2 and 15 μm and C_2H_4 from 10.5 to 11 μm. Where overlap appeared across the modeled regions, we added the optical depth values determined from earlier fits to the new regions (e.g., the best-fit optical depths for C_2H_2 and HCN were added to the optical depth for the C_4H_2, C_6H_2, HC_3N, and CH_3C_2H fits) and then performed the radiative transfer calculations. We expect that small errors may be introduced using this method, but due to the small difference in temperature between the layers, this effect should not be large.

Using the results from fitting the SH observations, we predicted the absorption in the SL data for benzene, C_2H_2, and C_4H_2. The CH_4 absorption was fit by itself between 7.5 and 7.9 μm, but the optical depth profiles for the $\nu_6 + \nu_8$ band of C_4H_2 as well as the C_2H_2 band at 7.5 μm as determined in the SH data were added to the total optical depth profile prior to calculating the radiative transfer calculations for the CH_4 fits.

5. RESULTS

The best fits for the SH and SL data are shown in Figure 2; the corresponding parameters are listed in Table 1. As can also be seen from the residuals in Figure 2, our models reproduce the observations quite well ($\chi^2_\nu \approx 0.84$ over the entire fitting region). Our best fits indicate that the molecules are found in a range of temperatures from 250 to 375 K; however, some of the temperature stratification may be artificial due to the large uncertainties on our temperature determinations.

5.1. Benzene

To fit the ν_4 bending mode of benzene at 14.85 μm, we require a high column density (log $N = 17.80$) consistent with the deep absorption in the spectrum. Our model reproduces the depth of the absorption feature well, but does not match the width and profile shape. This discrepancy is probably due to the absence of hot bands in our molecular model. Hot bands are generally slightly offset compared to the fundamental mode, and thus tend to broaden the absorption band. At the relatively high temperature of benzene found here, we certainly expect some contribution from the hot bands; at 300 K, only 54% of the molecules should be in the ground state (Kauppinen et al. 1980). However, hot bands are not included in the GEISA line list for benzene. As a result, our model fit is much narrower than it should be.

Using the benzene parameters found from fitting the ν_4 band, we predicted the appearance of the bands at 9.6 and 6.7 μm. As seen in Figure 2, while there are absorption features at these wavelengths consistent with benzene, our predictions do not fit these bands particularly well. At 9.6 μm, we can see that the predicted absorption is much deeper than the observed band, although the band shape is similar.

The feature at 6.7 μm is more unusual: while there is an overall absorption feature in the spectrum of SMP LMC 11 at this wavelength, the feature is much broader than our model and shows what could be a small emission bump right at the central wavelength of the benzene absorption. Just as for the 14.85 μm band, the broader observed feature could be a consequence of the absence of hot bands in our model. Indeed, we note that the absorption in the spectrum appears to be approximately twice as broad as in the model, with a similar red degraded wing (see Figure 3). Thus, we consider benzene the carrier for the overall absorption feature at 6.7 μm. The nature of the small emission bump is not clear. If this is a real emission feature, it seems unlikely that it would be due to benzene, since we do not see any similar emission at the other benzene absorption bands.

5.2. Acetylene Chains

The C_2H_2 absorption at 13.7 μm is the deepest and broadest absorption feature in the spectrum. Accordingly, we find the highest column density for this feature (log $N = 18.10$) of the molecular bands we fit. Since we ignored the deep and broad absorption between 12 and 16 μm, which is at least partly due to C_2H_2, this is clearly a lower limit of the true column density. In addition to the main isotopologue, we detect a fairly high column density of $H^{13}CCH$ (log $N = 16.90$) yielding an $N_{^{12}C_2H_2}/N_{H^{13}CCH}$ ratio of 16 and a $^{12}C/^{13}C$ ratio of 33. This is in the low end of the range for carbon-rich objects as determined by Milam et al. (2009), who found $^{12}C/^{13}C$ ratios between 25 and 90. However, since we underestimate the column density of the main isotopologue, this is most certainly an absolute lower limit to the $^{12}C/^{13}C$ ratio. Similarly, from the column densities of C_2H_2 and C_4H_2, we find a ratio of C_2H_2/C_4H_2 of 10, which would again be a lower limit.

We find that the identification of the ν_{11} band of C_6H_2 in this spectrum is uncertain. Using reasonable defringing techniques, the apparent absorption feature near 16.1 μm disappears (see Figure 4). Further, when the molecular constants from McNaughton & Bruget (1991) are used to calculate a model line list, we find that the calculated band center appears 0.02 μm longer of the apparent absorption in the spectrum. A comparison between our calculated model and the previously identi-

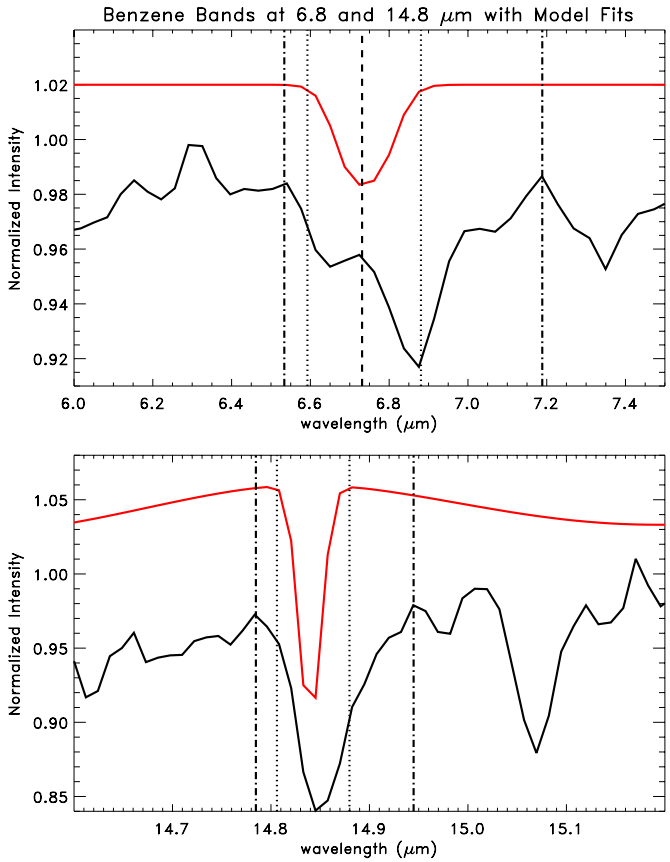

Figure 3. Benzene bands at 6.8 (top) and 14.8 μm (bottom), the spectra are in black while the benzene models are in gray (red). The dot-dashed vertical lines show the extent of the main absorption in the spectra, the dotted lines show the width of the model absorption for the entire band (at 6.8 μm) and for the Q-branch (at 14.8 μm). The dashed line in the top figure shows the center of the absorption, coincident with the emission at the center of the 6.8 μm band.

(A color version of this figure is available in the online journal.)

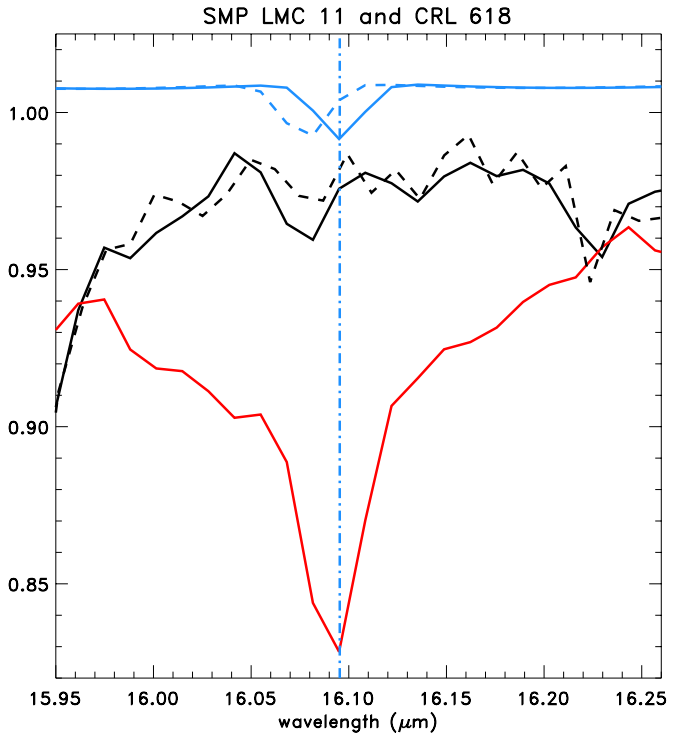

Figure 4. Normalized spectra of SMP LMC 11 (black) and CRL 618 (dark gray or red in the online version) are shown with the C_6H_2 models. The model calculated using molecular constants from McNaughton & Bruget (1991) is shown in the solid light gray (blue in the online version) lines, while the modified model is in dashed light gray (blue) lines. The band center for the model calculated with molecular constants from McNaughton & Bruget (1991) is highlighted with a light gray (blue) dot-dashed line. The dashed black line indicates an alternate fringing method for SMP LMC 11 wherein the appearance of the 16.07 μm feature is greatly diminished.

(A color version of this figure is available in the online journal.)

fied C_6H_2 absorption in CRL 618 (Cernicharo et al. 2001b) in Figure 4 indicates that our calculated model is at least correct in peak position, so we consider it possible that the apparent C_6H_2 absorption is not real.

If we assume that the peak near 16.07 μm is due to C_6H_2 and shift our model of this band accordingly, the best fit is obtained at $\log N = 15.60^{+0.70}_{-0.60}$, which does not reproduce the shape of the band. In order to fit the band shape, a $\log N$ of 16.30 is required. However, since we have to assume that the position of our band as well as our continuum choice is incorrect to obtain this result, it seems unlikely that this feature is actually C_6H_2.

5.3. Cyanopolyynes

Although there is no obvious absorption from HCN at 14 μm, our modeling attempts suggest that the overall fit is slightly better if HCN is included; in fact, we find a similar (low) column density for HCN as we do for the much stronger HC_3N. To verify whether the addition of HCN *significantly* improves the fit, we performed an F-test for an additional term (see Bevington & Robinson 2003). We find that for HCN, $F_\chi = 0.993$, and the probability of achieving this value for F_χ with the addition of a random factor in our model is 32%. Thus, HCN does not significantly improve the fit at this wavelength range and the column density we find should therefore be considered an upper limit. Thus, the upper limit for $HCN/HC_3N \approx 1$.

We do not detect any absorption at the position of the bending mode of HC_5N at 15.57 μm. Since the band strengths for the bending modes of HC_5N (268.2 cm^{-2} atm^{-1}; Bénilan et al. 2007) and HC_3N (245.1 cm^{-2} atm^{-1}; Jolly et al. 2007) are fairly similar and since the modes should have a similar profile, this suggests that HC_5N is simply not present in SMP LMC 11. From the measured equivalent width of the band (0.007 μm) and the S/N of ~85 in this part of the spectrum, we estimate an upper limit of $\log N = 15.4$ to the column density for HC_5N, yielding a lower limit to the HC_3N/HC_5N ratio of 10.

5.4. Other Species

Our best-fit model shows a clear contribution from CH_3C_2H at a relatively high column density, blended with the C_4H_2 absorption band. Again, we performed an F-test and found that in this case, adding CH_3C_2H does indeed significantly improve the fit: we find $F_\chi = 53$ and the probability of observing this F_χ value with the addition of a random factor is $\sim 10^{-8}$%. This absorption cannot be due to isotopologues of C_4H_2 either, as these absorb at longer wavelengths than the main isotopologue peak (at 15.95 and 15.93 μm for $H^{13}CCCCH$ and $HC^{13}CCCH$, respectively; Jolly et al. 2010). We thus conclude that CH_3C_2H is indeed present in the spectrum of SMP LMC 11. Note that this species was also observed in the pPN CRL 618 at millimeter wavelengths, and that it was suggested to contribute to the absorption at infrared wavelengths too (Cernicharo et al. 2001a). Here, however, we find a higher column density.

Finally, we also find good fits and fairly high column densities for the CH_4 absorption at 7.7 μm and the C_2H_4 absorption at 10.53 μm.

Judging from the residuals and low overall χ^2, we have accounted for most of the molecular absorption. Thus, any additional molecular bands apart from those already noted must be either weak or perhaps shallow and broad.

6. DISCUSSION

The rich molecular spectrum of SMP LMC 11 seems to offer a unique astrophysical laboratory to study chemical pathways in carbon-rich environments, including the formation of benzene. Indeed, although the CSE of SMP LMC 11 shares some properties with CRL 618—the only other pPN in which benzene is detected—there are some significant differences that offer clues to the conditions required for the efficient formation of benzene and other carbonaceous molecules.

6.1. Circumstellar Geometry

The first aspect we consider is the geometry of the CSE and the physical conditions of the material within. The continuum emission in the *Spitzer*–IRS observations is due to dust and provides the background intensity against which the molecular gas absorbs. Thus, the molecular gas is either mixed in with the dust or located further from the star. Additionally, the dust must be optically thick at infrared wavelengths to explain the overall shape of the combined SL and LL spectrum. Moreover, optically thick dust is consistent with the featureless shape of the dust continuum which can be represented reasonably well with blackbody curves (see also Section 3).

It is clear that the physical conditions in the CSE of SMP LMC 11 are somewhat different from those in CRL 618: the CSE of SMP LMC 11 is denser and warmer than that of CRL 618. We find a typical dust temperature of 425 K, whereas the dust temperature of CRL 618 is 98–110 K (Fonfría et al. 2011). Similarly, the molecular excitation temperatures are slightly higher—250–400 K versus 200–250 K—and we also find higher column densities (e.g., $N(C_2H_2) = 2 \times 10^{17}$ cm^{-2} in CRL 618, Cernicharo et al. 2001b, versus $\geqslant 10^{18}$ cm^{-2} in SMP LMC 11).

If the CSEs of both CRL 618 and SMP LMC 11 were simple outflows, the higher temperatures in SMP LMC 11 would indicate that the dust is located closer to the star and thus that SMP LMC 11 turned off the AGB more recently. Indeed, the dust and molecular gas temperatures in SMP LMC 11 are more typical of a late AGB star than a pPN for which dust temperatures of 150–300 K are expected (Kwok 2000). However, as seen in Figure 2, the *Spitzer*–IRS spectrum of SMP LMC 11 also exhibits weak emission from [Ne II], which is typically one of the first excitation lines seen in young PNe. This clearly indicates that the central star is much hotter than a typical AGB star and is thus in the pPN stage. This apparent contradiction is easily reconciled if we consider that the [Ne II] line does not originate from the same region as the molecular absorption and the dust. Indeed, since the dust is optically thick, the gas from which the [Ne II] originates cannot be located in a direct line of sight toward the central star: the dust hides the innermost region from view and no ionizing radiation can be expected to penetrate this thick dust layer. Thus, the [Ne II] line must originate from a region which is geometrically distinct from the location of the dust and the molecular gas and which is not obscured by dust.

The current results suggest that the molecular gas and dust surrounding SMP LMC 11 is located in a thick torus that we see fairly edge-on, as previously suggested in Paper I. In such a geometry, the gas that causes the [Ne II] emission would then be in a bipolar outflow. The properties of the central object thus correspond to those of a pPN, but the circumstellar material does not correspond to a pPN outflow and evolves on its own timescale since it resides in a massive disk. Such a disk with optically thick dust would also shield the circumstellar material from the intense radiation of the central object. Note that a radially constrained dusty torus could also explain why a dust model with a constant-velocity outflow at a constant mass-loss rate overestimates the flux at the longer wavelengths.

Thus, from the geometrical point of view, SMP LMC 11 is very similar to CRL 618 for which a similar geometry involving a dense torus (in addition to a bipolar outflow) is observationally established (see, e.g., Burton & Geballe 1986). Such massive, vertically extended and long-lived disks are often seen around binary systems containing an evolved star such as the Red Rectangle (see, e.g., Jura et al. 1995; Waters et al. 1998), for example. However, it is not clear what the primary cause for the higher temperatures in SMP LMC 11 is. This could simply indicate that the torus is closer to the central star than for CRL 618, either because the CSE is younger, or because it is expanding more slowly than that of CRL 618 (which is expanding at a rate of 20 km s^{-1}; see, e.g., Herpin & Cernicharo 2000). However, one could also attribute the different temperatures to differences in the optical thickness of the dust between the two objects. In either case, the molecular excitation seems constrained to a fairly small range in temperatures.

6.2. The Chemistry in SMP LMC 11

In terms of the molecular composition, the most striking difference between SMP LMC 11 and CRL 618 is the much stronger absorption that we find for benzene. The center of the benzene band at 14.85 μm is about three times deeper in SMP LMC 11 than in CRL 618. It may be somewhat surprising then that we find a column density that is 130 times larger than that found for CRL 618 (Cernicharo et al. 2001b); however, we believe that this difference is due to the fact that we used more recent line lists. Additionally, not only is benzene itself much more abundant in SMP LMC 11, it is also enhanced compared to most other species, especially compared to acetylene. If we take the lower limit for the column density of C_2H_2 at face value, we find that there is about twice as much C_2H_2 as there is benzene; for CRL 618, the ratio found between these molecules was about 40 (Cernicharo et al. 2001b).

The relative abundances of the acetylene chains might offer some hints about the chemistry leading to efficient benzene formation. Woods et al. (2002, 2003) found that the interstellar benzene formation route (McEwan et al. 1999) was not efficient in environments such as CRL 618. Instead, they proposed a much more efficient route in such environments starting from acetylene and HCO^+. The same model also predicts high column densities of C_4H_2 and C_6H_2 that are similar to one another. In fact, this matches the abundances in CRL 618 to within a factor 4–6. In the spectrum of SMP LMC 11, however, we cannot reliably establish the presence of C_6H_2 in the spectrum. This suggests that there is yet another formation route to benzene in these warm and dense environments, or possibly some additional reactions that need to be considered. These reactions might involve fast and efficient ring-closing reactions that deplete C_6H_2 or an additional route to benzene formation that starts

from the abundant C_2H_2 and C_4H_2 which then decreases the efficiency of the formation of C_6H_2.

It is equally interesting to consider the benzene loss reactions. Chemical models for environments comparable to those studied here show that the main destruction route for benzene is a further reaction with CN to form benzonitrile (C_6H_5CN; Woods et al. 2003). This molecular species has strong absorption bands at 13.2 and 14.4 μm, which we do not observe in the spectrum of SMP LMC 11. Although the CN in these reactions is expected to originate from the photodissociation of HCN, which is again at best marginally present in the spectrum of SMP LMC 11. Benzene destruction could thus be inhibited by the absence of the CN parent species.

The cyanopolyynes also present an interesting case. As shown in Cherchneff & Glassgold (1993), for example, the primary routes to the formation of cyanopolyynes in pPNe environments are through reactions between members of the acetylene family and the CN radical, which itself is produced from HCN in photochemical reactions. Reactions between CN and C_2H_2 then result in HC_3N, while reactions with C_4H_2 yield HC_5N. Since both C_2H_2 and C_4H_2 are abundant in the spectrum of SMP LMC 11, we would thus expect fairly large abundances of the longer cyanopolyynes as well. However, while we clearly detect a strong absorption band due to HC_3N, we do not find much evidence for the parent molecule, HCN, nor for the longer cyanopolyynes. HC_5N, for instance, should have a strong bending mode at 15.57 μm (Bénilan et al. 2007) which does not appear in the spectrum (see Figure 2).

Such abundance patterns are very different from those observed in CRL 618 and cannot be accommodated by the chemical models for these environments (e.g., Cherchneff & Glassgold 1993; Woods et al. 2003). Even if one were to consider that HCN could be completely depleted by HC_3N formation, one would expect to see efficient formation of HC_5N as well since this involves the same mechanism and large amounts of C_4H_2 are available for this process. This observation then suggests that for the cyanopolyynes, some of the chemical pathways that are possible in pPNe environments might be missing from the models.

6.3. Pathways to PAHs?

The formation of benzene is often studied in the context of PAHs, for which they are the basic unit. In the formation pathways for PAHs, the formation of benzene is considered to be the bottleneck (see, e.g., Allamandola et al. 1989). We searched for any features due to neutral naphthalene and pyrene (two of the smallest PAHs consisting of two and three aromatic rings, respectively) but did not find any evidence for these species. However, since PAH formation cannot occur at the low temperatures in SMP LMC 11—typically 900–1100 K is required (Frenklach & Feigelson 1989; Allamandola et al. 1989; Cherchneff et al. 1992), this should not be surprising.

It is interesting to consider what might happen to the benzene as the central star and CSE evolve further. All other things being equal, the increasingly hot central object would heat up the CSE. If the torus expands (as is the case for CRL 618), then the circumstellar material will become diluted and more transparent, which would clearly increase the importance of photochemistry. It is not immediately clear what the result of this increased photochemistry would be, but it is certainly possible that the conditions created are ideal for further processing of the circumstellar benzene into PAHs. If so, this might represent an important PAH formation pathway, provided that the torus contains enough mass to represent a significant carbon reservoir. Note that for objects like the Red Rectangle, the circumbinary disks are indeed found to be massive. However, in that particular object, PAHs are clearly found in the bipolar outflows (Waters et al. 1998) and not in the torus.

Although the molecular composition of the CSE of SMP LMC 11 is certainly unique thus far, we do not believe that the environment represented by this object is necessarily exceptional. CRL 618 is the only other source where benzene is detected, and it also shows different abundances for the polyynes and the cyanopolyynes. However, the two environments are very similar in many of their physical properties. Given the short expected timescales for the evolution from the tip of the AGB to the PN phase, it is reasonable to expect the evolution of CSEs to be fast. The two objects could then represent cases where either the initial conditions (of the torus, for example) were slightly different or, alternatively, they could represent slightly different steps in the evolution of the torus. It would certainly be interesting to study how the physical conditions of a (slowly expanding) dense torus change in this short evolutionary phase and how the chemistry in this environment will evolve.

7. CONCLUSIONS

We presented an analysis of the rich molecular absorption in the *Spitzer*–IRS spectrum of SMP LMC 11. We have compared it to chemical models for carbon-rich pPNe and to CRL 618, the only other pPN in which benzene is detected to date. The geometrical configuration in both objects is fairly similar and includes a dense, warm torus of material in which a rich molecular gas resides. However, the absolute and relative chemical abundances of the carbonaceous species in SMP LMC 11 do not match models and are also quite different from those in CRL 618. In particular, benzene is very abundant, making SMP LMC 11 an important environment to consider in the study of benzene and possibly also in PAH formation. Current chemical models can reproduce some of the molecular absorption, but not all of it. In particular, the absence of C_6H_2 and HC_5N seems to require additional ring-closing reactions that deplete those species. Alternatively, new chemical pathways have to be found for the formation of C_4H_2 and HC_3N that do not result in abundant formation of C_6H_2 and HC_5N. We encourage a more detailed study of the chemical pathways which could explain these anomalies.

S.E.M. acknowledges support from an Ontario Graduate Scholarship in Science and Technology (OGSST). J.C. is supported by the Spitzer Space Telescope General Observer program. This publication makes use of data products from the Two Micron All Sky Survey, which is a joint project of the University of Massachusetts and the Infrared Processing and Analysis Center/California Institute of Technology, funded by the National Aeronautics and Space Administration and the National Science Foundation. This research has made use of NASA's Astrophysics Data System Bibliographic Services and of the SIMBAD database, operated at CDS, Strasbourg, France. We also thank the anonymous referee for positive feedback and constructive comments which have improved the quality of this paper.

REFERENCES

Allamandola, L. J., Tielens, G. G. M., & Barker, J. R. 1989, ApJS, 71, 733
Arié, E., & Johns, J. W. C. 1992, J. Mol. Spectrosc., 155, 195

Bénilan, Y., Jolly, A., Trolez, Y., Raulin, F., & Guillemin, J. C. 2007, J. Mol. Spectrosc., 245, 109
Bernard-Salas, J., Peeters, E., Sloan, G. C., et al. 2006, ApJ, 652, L29
Bevington, P. R., & Robinson, D. K. 2003, Data Reduction and Error Analysis for the Physical Sciences (3rd ed.; New York: McGraw-Hill)
Burton, M. G., & Geballe, T. R. 1986, MNRAS, 223, 13P
Cami, J., van Malderen, R., & Markwick, A. J. 2010, ApJS, 187, 409
Cernicharo, J., Barlow, M. J., Gonzalez-Alfonso, E., et al. 1996, A&A, 315, L201
Cernicharo, J., Heras, A. M., Pardo, J. R., et al. 2001a, ApJ, 546, L127
Cernicharo, J., Heras, A. M., Tielens, A. G. G. M., et al. 2001b, ApJ, 546, L123
Cherchneff, I., Barker, J. R., & Tielens, A. G. G. M. 1992, ApJ, 401, 269
Cherchneff, I., & Glassgold, A. E. 1993, ApJ, 419, L4
Cutri, R. M., Skrutskie, M. F., van Dyk, S., et al. 2003, The IRSA 2MASS All-Sky Point Source Catalog, NASA/IPAC Infrared Science Archive (Pasedena, CA: Caltech)
Dang-Nhu, M., & Plíva, J. 1989, J. Mol. Spectrosc., 138, 423
Dopita, M. A., Meatheringham, S. J., Webster, B. L., & Ford, H. C. 1988, ApJ, 327, 639
Fonfría, J. P., Cernicharo, J., Richter, M. J., & Lacy, J. H. 2011, ApJ, 728, 43
Frenklach, M., & Feigelson, E. D. 1989, ApJ, 341, 372
Guelachvili, G., Craig, A. M., & Ramsay, D. A. 1984, J. Mol. Spectrosc., 105, 156
Herpin, F., & Cernicharo, J. 2000, ApJ, 530, L129
Higdon, S. J. U., Devost, D., Higdon, J. L., et al. 2004, PASP, 116, 975
Houck, J. R., Roellig, T. L., van Cleve, J., et al. 2004, ApJS, 154, 18
Iben, I., Jr., & Renzini, A. 1983, ARA&A, 21, 271
Jacquinet-Husson, N., Scott, N. A., Chédin, A., et al. 2008, J. Quant. Spectrosc. Radiat. Transfer, 109, 1043
Jolly, A., Benilan, Y., & Fayt, A. 2007, J. Mol. Spectrosc., 242, 46
Jolly, A., Fayt, A., Benilan, Y., et al. 2010, ApJ, 714, 852
Jura, M., Balm, S. P., & Kahane, C. 1995, ApJ, 453, 721
Kauppinen, J., Jensen, P., & Brodersen, S. 1980, J. Mol. Spectrosc., 83, 161
Khlifi, M., Paillous, P., Delpech, C., et al. 1995, J. Mol. Spectrosc., 174, 116
Kwok, S. 2000, The Origin and Evolution of Planetary Nebulae (Cambridge Astrophysics Series 33; Cambridge: Cambridge Univ. Press)
Latter, W. B. 1991, ApJ, 377, 187
Lebouteiller, V., Bernard-Salas, J., Sloan, G. C., & Barry, D. J. 2010, PASP, 122, 231
McEwan, M. J., Scott, G. B. I., Adams, N. G., et al. 1999, ApJ, 513, 287
McNaughton, D., & Bruget, D. N. 1991, J. Mol. Spectrosc., 150, 620
Milam, S. N., Woolf, N. J., & Ziurys, L. M. 2009, ApJ, 690, 837
Morgan, D. H. 1984, MNRAS, 208, 633
Morgan, D. H., & Parker, Q. A. 1998, MNRAS, 296, 921
Rothman, L. S., Gordon, I. E., Barbe, A., et al. 2009, J. Quant. Spectrosc. Radiat. Transfer, 110, 533
Sanduleak, N., MacConnell, D. J., & Philip, A. G. D. 1978, PASP, 90, 621
Shaw, R. A., Stanghellini, L., Villaver, E., & Mutchler, M. 2006, ApJS, 167, 201
Skrutskie, M. F., Cutri, R. M., Stiening, R., et al. 2006, AJ, 131, 1163
Snow, T. P., & Witt, A. N. 1995, Science, 270, 1455
Speck, A. K., Cami, J., Markwick-Kemper, C., et al. 2006, ApJ, 650, 892
Vassiliadis, E., & Wood, P. R. 1994, ApJS, 92, 125
Waters, L. B. F. M., Cami, J., de Jong, T., et al. 1998, Nature, 391, 868
Werner, M. W., Roellig, T. L., Low, F. J., et al. 2004, ApJS, 154, 1
Western, C. M. 2010, PGOPHER, A Program for Simulating Rotational Structure (Bristol: Univ. Bristol), http://pgopher.chm.bris.ac.uk/
Woods, P. M., Millar, T. J., Herbst, E., & Zijlstra, A. A. 2003, A&A, 402, 189
Woods, P. M., Millar, T. J., Zijlstra, A. A., & Herbst, E. 2002, ApJ, 574, L167